



**HAL**  
open science

## Design of tailored oxide-carbide coating on carbon fibers for a robust copper/carbon interphase

Loic Constantin, Lisha Fan, Qiming Zou, Benjamin Thomas, Jérôme Roger,  
Jean-Marc Heintz, Catherine Debiemme-Chouvy, Bruno Mortainge, Yong  
Feng Lu, Jean-François Silvain

### ► To cite this version:

Loic Constantin, Lisha Fan, Qiming Zou, Benjamin Thomas, Jérôme Roger, et al.. Design of tailored oxide-carbide coating on carbon fibers for a robust copper/carbon interphase. *Carbon*, 2020, 158, pp.607-614. 10.1016/j.carbon.2019.11.032 . hal-02361314

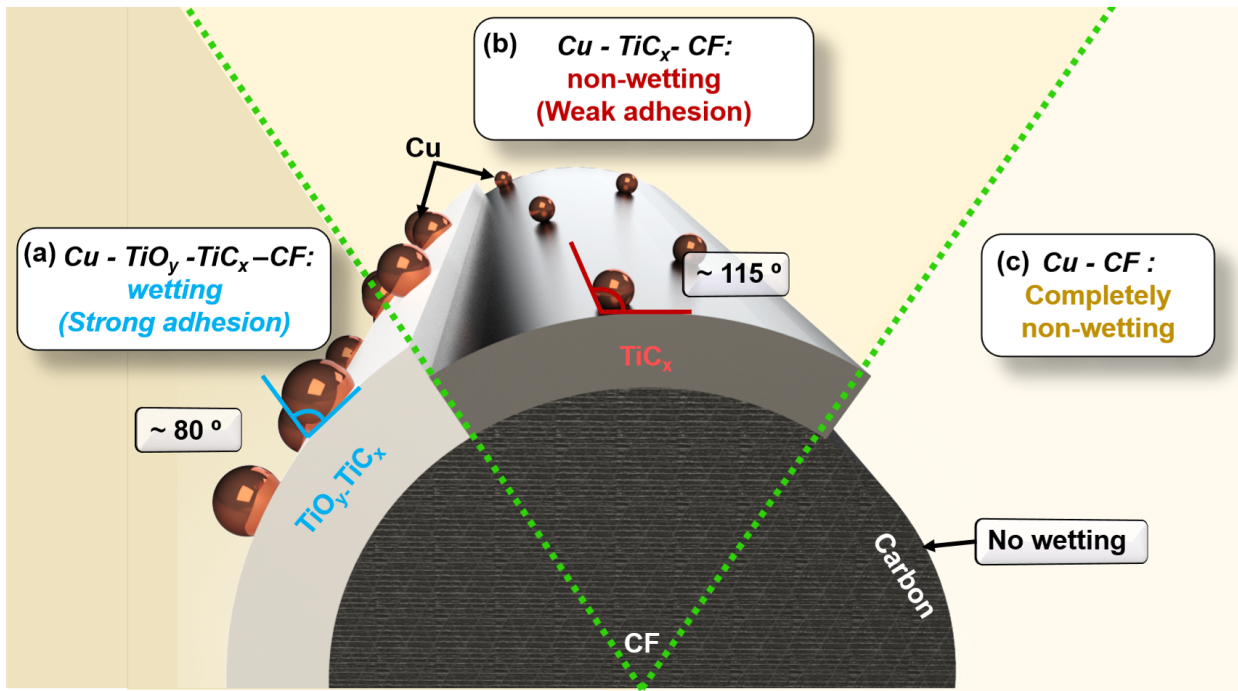
**HAL Id: hal-02361314**

**<https://hal.science/hal-02361314>**

Submitted on 14 Nov 2019

**HAL** is a multi-disciplinary open access archive for the deposit and dissemination of scientific research documents, whether they are published or not. The documents may come from teaching and research institutions in France or abroad, or from public or private research centers.

L'archive ouverte pluridisciplinaire **HAL**, est destinée au dépôt et à la diffusion de documents scientifiques de niveau recherche, publiés ou non, émanant des établissements d'enseignement et de recherche français ou étrangers, des laboratoires publics ou privés.



## **Design of Tailored Oxide-Carbide Coating on Carbon Fibers for a Robust Copper/Carbon Interphase**

*Loic Constantin,<sup>1,2,‡</sup> Lisha Fan,<sup>2,‡</sup> Qiming Zou,<sup>2</sup> Benjamin Thomas,<sup>1</sup> Jérôme Roger,<sup>3</sup>  
Jean-Marc Heinz,<sup>1</sup> Catherine Debiemme-Chouvy,<sup>4</sup> Bruno Mortainge,<sup>5</sup> Yong Feng Lu,<sup>2,\*</sup> and  
Jean-Francois Silvain<sup>1,2,\*</sup>*

<sup>1</sup> CNRS, Univ. Bordeaux, Bordeaux INP, ICMCB, UMR 5026 F-33608 Pessac, France.

<sup>2</sup> Department of Electrical and Computer Engineering, University of Nebraska-Lincoln, Lincoln, NE, 68588.

<sup>3</sup> Université de Bordeaux, Laboratoire des Composites Thermo Structuraux – LCTS 3 allée de la Boétie, F-33600 Pessac Cedex, France.

<sup>4</sup> Laboratoire Interfaces et Systèmes Electrochimiques – LISE, UMR 8235, CNRS, Sorbonne Université, 4 place Jussieu F-75252 Paris Cedex, France.

<sup>5</sup> Département Générale de l'Armement - DGA/DS/Mission pour la Recherche et l'Innovation Scientifique, 92221 Bagneux, France.

\* Corresponding Authors, Jean-Francois Silvain: [jean-francois.silvain@icmcb.cnrs.fr](mailto:jean-francois.silvain@icmcb.cnrs.fr) and Yong Feng Lu: [ylu2@unl.edu](mailto:ylu2@unl.edu)

**Abstract:** The lack of robust interphases between carbon and most metals prevent the exploration of the full scope potential of carbon-based metal matrix composites. Here, we demonstrated a scalable and straightforward way to produce strong interphase between copper (Cu) and carbon fibers (CFs) by designing a tailored titanium oxide-carbide coating ( $\text{TiO}_y\text{-TiC}_x$ ) on CFs in a molten salt process. The oxide-carbide composition in the graded layer strongly depends on the coating temperature (800-950 °C). A coating with a high  $\text{TiO}_y$  content obtained at a low coating temperature (800 °C) contributes to better molten-Cu wetting and strong adhesion energy between CFs and Cu during a subsequent exposure at 1200 °C. The Cu wetting angle for the  $\text{TiO}_y\text{-TiC}_x\text{-CF}$  sample obtained at 800 °C was  $\sim 80^\circ \pm 5^\circ$  with a Cu surface coverage of  $\sim 50\%$  versus  $\sim 115^\circ$  and  $\sim 10\%$  for the  $\text{TiC}_x\text{-CF}$  sample made at 950 °C. The kinetic analysis of the coating process step by step suggests a growth rate limited by the mass-transfer through the coated layer. This method provides a novel approach to improve the thermal conductivity of Cu/C composite for thermal management applications.

## 1. INTRODUCTION

Metal matrix composites (MMC) need robust interphases to enhance mechanical adhesion and tailor the overall properties of the resultant composite [1]. The formation of interphases is particularly crucial in composites comprised of chemically and thermomechanically dissimilar compositions [2,3]. Copper (Cu) reinforced carbon fibers (CFs) is an excellent example of MMC with weak interfacial bonding. This MMC is of particular interest in thermal management, as a next-generation heat sink material [4]. Solid Cu alone is limited by fatigue failure due to cyclical thermal stresses. Adding CFs to reinforce Cu offers one advantage of combining the high strength, low fatigue failure of CFs with the high thermal conductivity of Cu ( $400 \text{ W}\cdot\text{m}^{-1}\text{K}^{-1}$ ). Nevertheless, a simple Cu-CFs composite suffers from poor Cu wettability on carbon (C) due to

the lack of chemical affinity [5]. The lack of affinity is more significant when molten metal is in direct contact with the carbon reinforcement such as in gas pressure infiltration, squeeze casting, stir casting, or more recently laser printing [6–8].

Extensive experimental and theoretical work has been devoted on the interphase engineering to improve CF-reinforced Cu matrix composite [9,10]. One approach has been to alloy the metal with carbide-forming elements (e.g., titanium (Ti), zirconium (Zr), chromium (Cr), and boron (B)) [11–13]. However, the properties are severely degraded due to inhomogeneous dispersion of the alloying elements at the interface [14–16]. The second approach of considerable interest is to coat the carbon reinforcement with carbides [17,18]. Titanium carbide (TiC) offers strong oxidation resistance, high mechanical strength, excellent chemical stability, and low density, making it a right candidate as interphase [19]. However, it has been reported that TiC does not wet thoroughly molten Cu (contact angle  $>115^\circ$ ), resulting in poor adhesion to TiC surfaces [20].

This paper reports a third approach, which consists of creating a graded titanium oxide - carbide ( $\text{TiO}_y\text{-TiC}_x$ ) coating on CFs using a molten-salt method to tailor the Cu – Carbon interphase. Molten-salt synthesis provides a versatile and efficient way to produce transition metal carbides at relatively low temperatures in short time frames. The salt acts as a solvent to dissolve the metal powders and, therefore, enhance the Ti mass transport to the CF surfaces [21,22]. The research results showed that the presence of a thin  $\text{TiO}_y$  outer layer on the  $\text{TiC}_x$  coating improves the wettability of molten Cu (**Figure 1**). The interfacial wetting angle of Cu on the  $\text{TiO}_y\text{-TiC}_x$ -coated CFs reduced to be  $\sim 80 \pm 5^\circ$ , thus offering a significant improvement over  $\text{TiC}_x$  alone. The rate of elemental diffusion and the nature of the Cu- $\text{TiO}_y$  and Cu- $\text{TiC}_x$  bonding were examined. The influence of the coating temperature and time on the  $\text{TiO}_y\text{-TiC}_x$  microstructures and the chemical compositions of the coatings were quantified. Finally, the process kinetics showed that

the mass-transfer limits the rate of  $TiC_x$  formation through the coated layer; the effective diffusivities governing the process were determined.

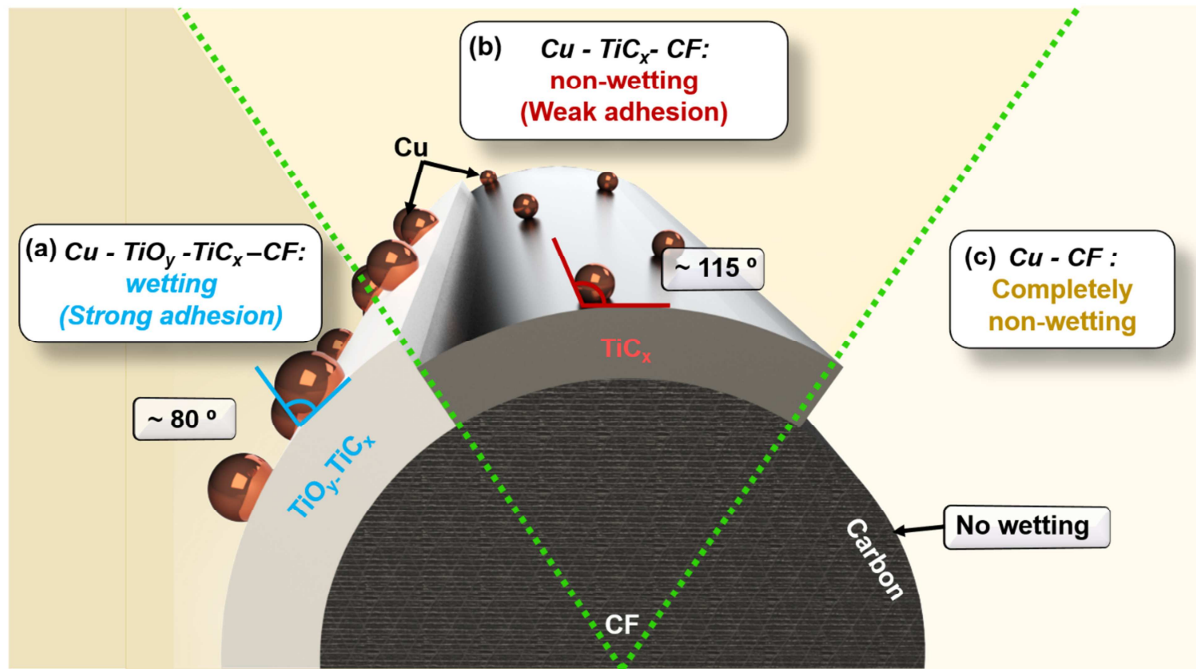


**Figure 1.** Schematic illustration of Cu wetting behavior measured by contact angles and droplet coverage on CFs with different interphases: (a)  $TiO_y-TiC_x$ , (b)  $TiC_x$ , and (c) bare CF.

## 2. EXPERIMENTAL SECTION

### 2.1. Preparation of coatings on CFs.

The synthesis of the carbide coatings was carried out by a molten-salt process, illustrated schematically in **Figure 2**. First, CFs (Mitsubishi Chemical DIALEAD™ K223HM) were mixed with a potassium chloride (KCl) (GPR Rectapur® 99%) salt and metallic Ti powder (Ti 99.5%, mean diameter 40  $\mu m$ ) at a molar ratio of  $KCl:C:Ti = 0.64:1:0.125$ . The mixture was then placed in alumina ( $Al_2O_3$ ) crucible and heated in a tube oven filled with flowing argon (Ar) gas. The coating temperature varied from 800 to 950 °C for times of up to 5 h. These coating conditions were chosen based on Lui *et al.* study [23]. After cooling down, the crucible was immersed in a

boiling distilled water ( $\sim 100\text{ }^{\circ}\text{C}$ ) until the salt was fully dissolved. Finally, the coated CFs were filtered from the solution, flushed with deionized (DI) water, and air-dried in an oven at  $60\text{ }^{\circ}\text{C}$  for 1 h. The filtration dissolution/filtering process was repeated three times; the coated CF product yield is  $\sim 95\%$ .



**Figure 2.** Schematic illustration of the molten-salt process for preparing TiC-based coatings on CFs.

### 2.2. Wettability analysis.

The wettability of molten Cu (melting point  $1085\text{ }^{\circ}\text{C}$ ) on the coated CFs was investigated using an approximate equal-molar mixture of  $0.2\text{ g}$  ( $\sim 0.017\text{ mol}$ ) of coated CFs with  $1.2\text{ g}$  ( $0.019\text{ mol}$ ) of dendritic Cu powder ( $35\text{ }\mu\text{m}$ , ECKA Granules Germany CmbH). The mixture was placed in an  $\text{Al}_2\text{O}_3$  crucible with a carbon paper liner to prevent reaction between the Cu powder and the crucible. The crucible was put into a tube oven filled with flowing argon gas and heated to  $1200\text{ }^{\circ}\text{C}$  with a rate of  $10\text{ }^{\circ}\text{C}/\text{min}$ . The crucible was held for 10 min and then cooled to room temperature at a rate of  $15\text{ }^{\circ}\text{C}/\text{min}$ . Contact angles between the CFs and the Cu droplets were

determined using scanning electron microscopy (SEM) and cross-sectional images of resin-encased and polished CFs.

### ***2.3. Quenching tests.***

Rapid thermal quenching of the molten salt in the ambient air was used to terminate the coating process at intermediate stages. This enabled the study of the TiC formation, including Ti dissolution, diffusion, and reaction with CFs. The quenching tests were performed by heating the powder mixture to 800 and 950 °C for 0.5 and 5 h, respectively. The hot crucible was then rapidly quenched in the air at a cooling rate of about 500 °C/min, resulting in KCl ( $m_p = 770^\circ\text{C}$ ) solidification in less than 20 s. A piece of the solidified KCl-CFs-Ti sample was embedded in a polyphenolic resin, and mechanically dry polished for SEM analyses.

### ***2.4. The growth rate of the TiC layer.***

The diffusivity and associated activation energy were measured by mixing KCl, CFs, and Ti with a molar ratio of KCl:CFs: Ti = 0.642:1:0.238. Both coating times and temperatures were varied between 1 to 5 h at processing temperatures of 800, 850, 900, and 950 °C, respectively. After the reaction, the coated CFs were washed and dried as described earlier. The coated CFs were then embedded in a polyphenolic resin and polished for SEM analyses.

### ***2.5. Characterization methods.***

Morphological and microstructural characterization was performed using an SEM (VEGA II SBH, TESCAN). Crystal structures and chemical phases were identified by X-ray diffraction (XRD) (PANalytical X'pert PRO MPD,  $\lambda = 1.5405 \text{ \AA}$ ). The stoichiometry of  $\text{TiC}_x$  was estimated by calculating the lattice parameters from the XRD diffractograms via the Le-Bail method [24] using the FullProf Suite. Auger electron spectroscopy (AES) (Auger VG Scientific Microlab

310F) and X-ray photoelectron spectroscopy (XPS, Thermo Electron K-alpha photoelectron spectrometer, Al K $\alpha$  excitation) were used to determine the elemental and chemical compositions. The AES sputtering time was converted to a depth profile by measuring the layer removal depth using SEM. Grain morphology, orientation, and size were evaluated using electron backscatter diffraction (EBSD).

### 3. RESULTS AND DISCUSSION

#### 3.1. Effect of temperature on TiC<sub>x</sub> coating composition and morphology

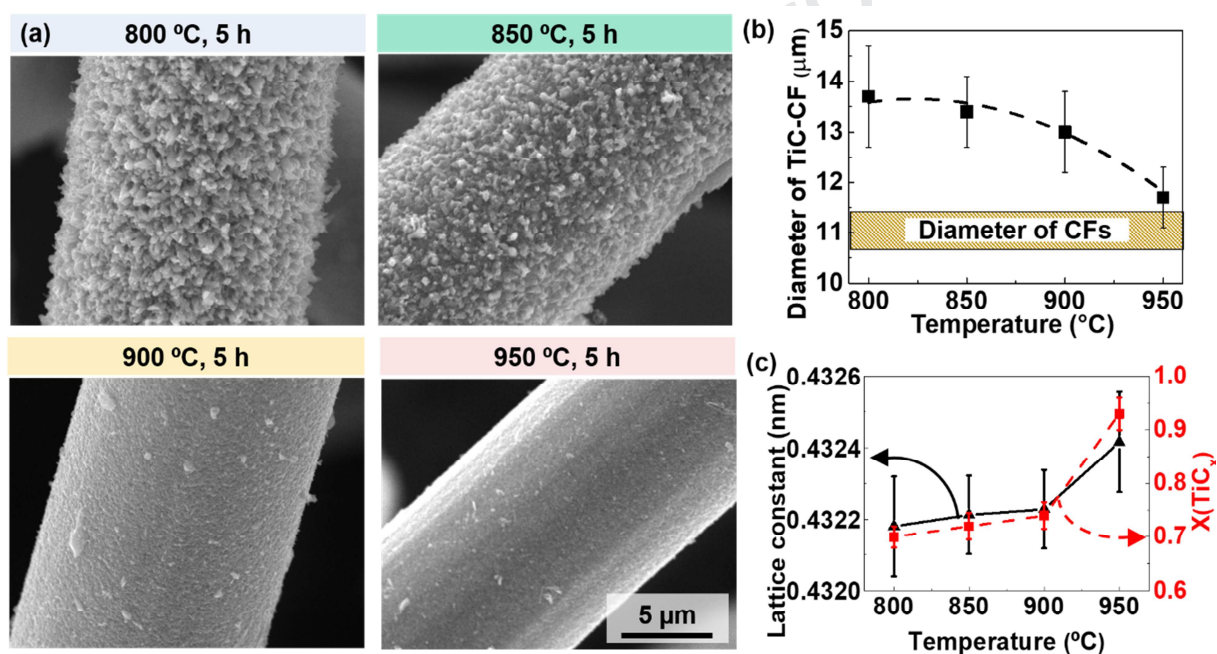


**Figure 3.** Influence of the coating temperature, ranging from 800 to 950 °C, on the layer morphology and composition, **a)** SEM micrographs, **b)** TiC<sub>x</sub>-CF diameter vs. coating temperature, and **c)** measured lattice constant and associated C/Ti atomic ratio vs. temperature.

The effects of reaction temperature on the coating morphology and structure are shown in **Figure 3**. In this study, the reaction time was 5 h at temperatures ranging from 800 to 950 °C. The SEM micrographs of the coatings (**Figure 3 (a)**) display a dramatic change in the morphology with

different temperatures. Specifically, at 800 and 850 °C, the surfaces appeared to be a porous collection of particle-like features with open, interconnected porosity of more than 50% (pore sizes from 300 to 1000 nm). This suggests the growth was from reactive C surface sites with little consolidation by surface-diffusion-driven sintering. Both Xiaoguang Liu *et al.* [23] and Qian Liu *et al.* [25] have observed similar porous coatings formed by Ti reaction with carbon substrates at 750 °C in a potassium chloride:lithium chloride (KCl:LiCl) salt and at 900 °C in a lithium chloride:potassium chloride:potassium fluoride (LiCl:KCl:KF) salt, respectively.

In contrast, coatings at 900 and 950 °C have far fewer and smaller pores and appear almost fully consolidated. In these cases, the temperature is sufficiently high that localized differences in surface reactivity become less critical for determining the growth morphology. Moreover, the possibility of sintering driven by surface diffusion would be more significant. Both effects, individually or combined, could explain the dense coating obtained at high temperatures. Others have reported consolidated coatings at temperatures above 900 °C in different salts [18,26].

Scanning electron micrographs show that the diameters of the reacted fibers (*i.e.*, core CFs plus coated layers) decreased as the temperature increased, as plotted in **Figure 3 (b)**. In other words, the growth of porous coatings at 800 and 850 °C caused the resulting diameter to increase from ~11 (*i.e.*, original CFs) to 13  $\mu\text{m}$  (*i.e.*, coated CFs). In contrast, the layer obtained at 950 °C was almost fully dense and increased the product diameter by only ~0.5  $\mu\text{m}$  from the original CF diameters. The coating porosity was estimated from a mass balance of the reactants, as given in the Supplementary Information (SI), Section 2. The fully dense (0% porosity) coating thickness was predicted to be 0.55  $\mu\text{m}$  via the mass balance calculation, suggesting an outer fiber diameter of 11.45  $\mu\text{m}$ . This is in reasonable agreement with the outer diameter of 11.6  $\mu\text{m}$  observed for fibers reacted at 950 °C (**Figure 3 (b)**) and supported the observations that the porosity was low

(<10%). Similarly, the coating prepared at 800 °C has a measured outer diameter of ~13.5 μm, suggesting a porosity of ~65%, again in agreement with the observations.

In addition to the surface morphology, XRD was performed at each processing temperature to quantify the product phase composition (**Figure S1 (c)**). The relationships between the  $\text{TiC}_x$  lattice parameters and the coating temperature were determined from XRD data using the Le-Bail method (**Figure 3 (c)**).[24] Further details from the analyses are provided in **Figure S2**. A correlation between the  $\text{TiC}_x$  lattice parameters and the chemical stoichiometry was established to determine the change in the coating stoichiometry as a function of the temperature [27–29]. The results show, within the experimental errors, that the stoichiometry is  $\sim\text{TiC}_{0.73}$  for the product formed between 800 to 900 °C. On the other hand, the coating produced at 950 °C has a higher carbon content with a stoichiometry of  $\sim\text{TiC}_{0.93}$ . One explanation for the change is that the Ti and C diffusivities were both greater at higher temperatures and thus tended to form a more reacted coating. This explanation is supported in part by the measurements of the self-diffusion coefficients of C and Ti in TiC as a function of the temperature [30–32], as well as results from the process kinetics, described later in this work.

### 3.2. Interphase elemental composition ( $\text{TiC}_x$ vs. $\text{TiO}_y\text{-TiC}_x$ )

In the previous section, it was shown that the salt bath temperature influenced the morphology and stoichiometry of the  $\text{TiC}_x$  coating. This section describes how a combination of SEM, AES, and XPS was used to quantify the chemical compositions of the coated layers produced at the low (800 °C) and high (950 °C) temperatures. The AES compositional mapping in **Figure 4** shows the presence of not only  $\text{TiC}_x$  on the CF surfaces but also an outer layer of  $\text{TiO}_y$ . The elemental analyses at different depths of the coatings prepared at 800 °C show a *thin*  $\text{TiO}_y$  outer layer that extends to a depth of ~20% of the coating thickness. Based on the results in **Figure 4**

(a), the width of the 800 °C coating is about 1.2  $\mu\text{m}$ , suggesting an outer partially oxidized layer of 250 nm. In contrast, the coatings prepared at 950 °C were significantly denser with a thickness of  $\sim 0.30 \mu\text{m}$  (Figure 4 (b)) and a  $\text{TiO}_y$  outer layer of  $< 5 \text{ nm}$ . In other words, the 950 °C coating is essentially 100%  $\text{TiC}_x$ . Supplementary details of the AES are provided in Figure S3.

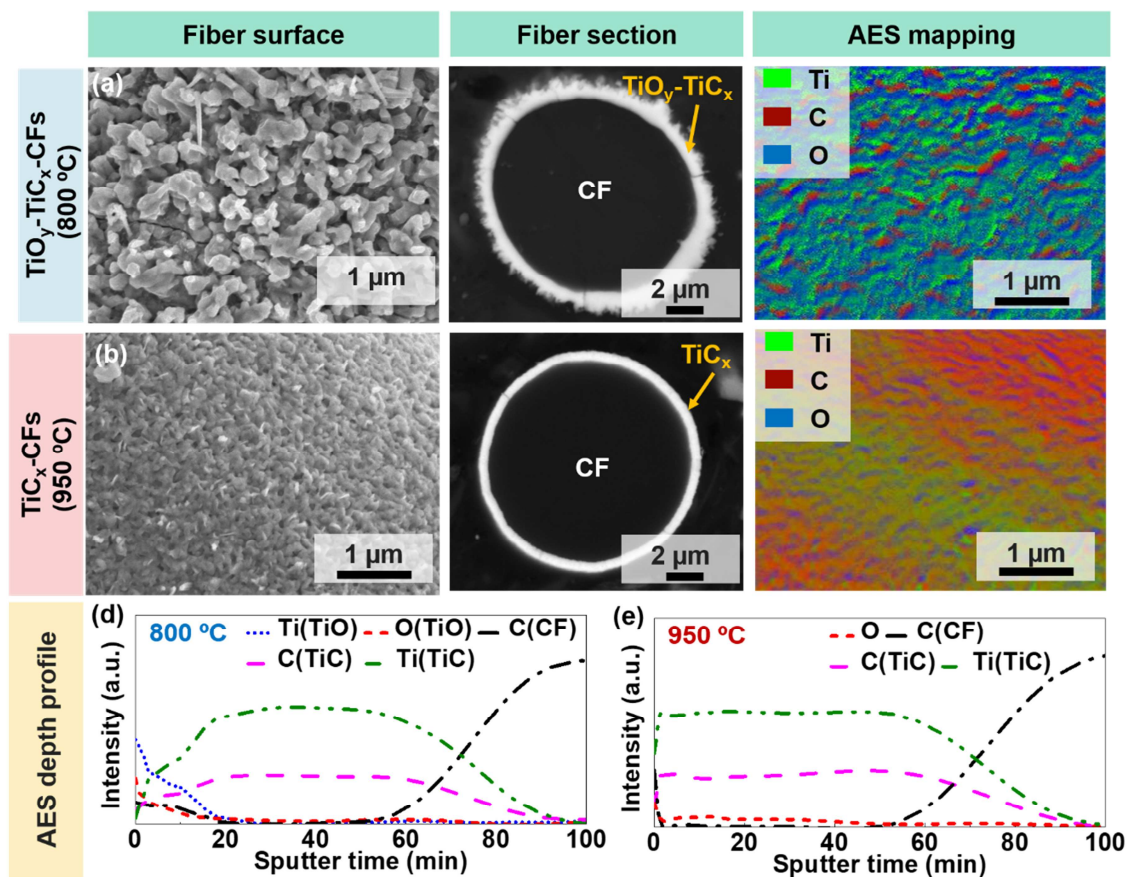


**Figure 4.** Surface morphology, cross-sectional and AES maps of the coated CFs prepared at (a) 800 and (b) 950 °C, respectively; and AES depth profiles of the coated CFs prepared at (d) 800 and (e) 950 °C, respectively.

Additionally, XPS was used to quantify the influence of the coating temperature on the graded oxide-carbide ratio. The C-C peaks observed at the binding energy (BE) of 284.6 eV in the C 1s spectra, originated from the unreacted CFs. The O 1s spectrum shows an O=C peak (BE  $\sim 530$  eV).

eV) with an O-Ti shoulder (BE ~ 531 eV); and the Ti 2p spectra shows two types of bonding configurations: Ti-C and Ti-O, respectively (**Figure S4**). Standard spectral analysis procedures were used to separate the XPS Ti 2p spectra into contributions from  $\text{TiC}_x$  and  $\text{TiO}_y$  (**Table 1**). The results display the same trend as the AES results: the distributions of surface Ti bonded as Ti-C vs. Ti-O strongly depend on the coating temperature. The results demonstrate ~50% of the surface Ti was bonded as  $\text{TiO}_y$  at 800 °C with only ~10% at 950 °C.

**Table 1.** XPS quantitative analyses using peak integration.

Sample	$C_{\text{tot}}$ (at %)	$C_{\text{TiC}_x}$ (at%)	$Ti_{\text{tot}}$ (at %)	$Ti_{\text{TiO}_y}$ (at %)	$Ti_{\text{TiO}_y}$ (%)	$Ti_{\text{TiC}_x}$ (%)
$\text{TiO}_y\text{-TiC}_x\text{-CFs}$ (800 °C)	70.8	7.3	14.6	7.3	50	50
$\text{TiC}_x\text{-CFs}$ (950 °C)	70.8	13.2	14.5	1.5	10.3	89.7

The presence of  $\text{TiO}_y$  was unexpected as the Ti + CF reaction was carried out in a flowing Ar gas. A possible explanation is that the  $\text{TiO}_y$  formed during boiling water (~100 °C) dissolution of the KCl salt at the end of the process. Naturally, the effective oxidation depth (via both the AES and XPS) would be larger for the highly porous coatings obtained at 800 °C simply due to the enhanced water penetration. Also, the coatings obtained at 800 °C have a more stoichiometrically Ti-rich layer ( $\text{TiC}_{0.73}$ , see the previous section), suggesting more reactive, non-bonded Ti sites that could be oxidized. In contrast, the highly consolidated and essentially pure  $\text{TiC}_x$  coatings formed at 950 °C (i.e.,  $\text{TiC}_{0.93}$ ) would encounter much less water penetration and, thus, less oxidation.

### 3.3. Cu wettability and interphase surface energy

To establish the role of a graded  $\text{TiO}_y\text{-TiO}_x$  coating to tailor the interfacial bonding between Cu and C, we prepared two types of CFs coated with a high and a low concentration of oxide content, respectively. The contact angles (wettability) of Cu on coated CFs prepared at 800, and 950 °C were measured, and the well-known Young-Dupre equation was used to estimate the adhesion energy:

$$E_{SL} = \gamma_{LV}(1 + \cos \theta), \quad (5)$$

where  $E_{sl}$  is the energy (work) of adhesion ( $\text{mN}\cdot\text{m}^{-1}$ ),  $\gamma_v$  is the liquid/vapor surface energy (tension) ( $\text{mN}\cdot\text{m}^{-1}$ ), which has been reported to be  $\gamma_{Cu} = 1257 - 0.2(T - 1356)$  for Cu [33], and  $\theta$  is the equilibrium contact angle. The results show that Cu does not wet CFs due to the low surface energy of the material (supplementary **Figure S5**). This is in agreement with the prior work reporting a contact angle of 145° [34]. Creation of a TiC coating on CFs has shown to reduce the Cu contact angle to 115° [35], but the coating is still *nonwetting* and is confirmed in this study for a coating prepared at 950 °C (**Figures 5 (a)** and **(c)**). In contrast, the coated CFs prepared at 800 °C, with  $\text{TiO}_y$  layer (**Figures 5 (b)** and **(c)**), show a Cu wetting angle of  $\sim 80^\circ$  ( $\pm 5^\circ$ ) and thus is a good wetting surface. In other words, there was sufficient oxide on the outer surface to increase the coating surface energy. For comparison, data reported for a Cu wetting angle of 80° on TiO is also included (**Figure 5 (c)**) [36].

Recall that the  $\text{TiO}_y\text{-TiC}_x$  coatings prepared at 800 °C are highly porous (**Figure 5 (a)**). However, after heating at 1200 °C during the Cu wetting tests, the surface fully consolidated (**Figure 5 (d)** and **(f)**). The surface coverage by Cu droplets on the coated and bare CFs (**Figure S6**) was computed and compared with the fraction of  $\text{TiO}_y$  in the coatings (**Figure 5 (h)**). The Cu coverage was fivefold greater on  $\text{TiO}_y\text{-TiC}_x$  CFs compared to the  $\text{TiC}_x$  CFs and. As expected, the Cu coverage of the bare (unreacted) CFs was negligible. The transition from low to high

wettability correlates perfectly with the steady increase of  $\text{TiO}_y$  content in the  $\text{TiC}_x$  coatings. The improved Cu wettability achieved with the graded  $\text{TiO}_y\text{-TiC}_x$  coatings developed in this work suggests a rather simple processing pathway for producing robust interphase in metal-carbon composites. The simplicity and cost-effectiveness of a molten salt process have been extensively used to prepare a TiC interphase in Cu/C composites. Often high coating temperature is employed, resulting in the formation of a pure TiC layer [17,25]. As demonstrated previously, TiC is known as a *nonwetting* element on molten Cu with a contact angle of 115 °. The development of a tailored  $\text{TiO}_y\text{-TiC}_x$  enables the formation of strong interphase between Cu and C in comparison to a pure TiC layer. The strong interfacial bonding observed in this work between the graded  $\text{TiO}_y\text{-TiC}_x$  layer and Cu will indubitably enhance the interaction between molten Cu and coated-CFs during the composite fabrication via gas infiltration, stir casting, squeeze casting or more recently, selective laser melting [6,7].

#### ***3.4. The kinetic analysis of the coating formation process***

To further understand the formation process of the graded coating, the molten salt was rapidly quenched at intermediate stages to "freeze" the state of the reaction to examine the intermediate states (**Figure S7**). Three steps mainly govern the growth process: 1) oxidation-driven dissolution of Ti particles into the salt ( $\text{Ti}^0$  to  $\text{Ti}^{n+}$ ), [37,38] 2) diffusion mass transport of  $\text{Ti}^{n+}$  to the surface of the CFs or the  $\text{TiC}_x\text{-CF}$  interphase, and 3) Ti and C mass transport through the  $\text{TiC}_x$  interphase layer and reaction (**Figure 6 (a)**). In the analyses below, the characteristic times for the three process steps ( $t_1$ ,  $t_2$ , and  $t_3$ , respectively) are estimated and compared to determine which is the rate-limiting factor in the coating process.

Regarding Ti dissolution (Step 1), the intermediate state of the Ti particles in the sample that was heated at 800 °C for 0.5 h and then quenched was observed. The results show that the original 40

$\mu\text{m}$  Ti particles had not only begun to dissolve but also showed significant disintegration into small sub-particles (presumably individual Ti grains) (**Figure 6 (b)**). The computation in SI section 3 shows that the particular dissolution time for an isolated Ti particle in an infinite bath of KCl is about  $\sim 4$  min. Thus, it can be concluded that the Ti dissolution rate is fast and rapidly saturates the small KCl volume used in these tests.

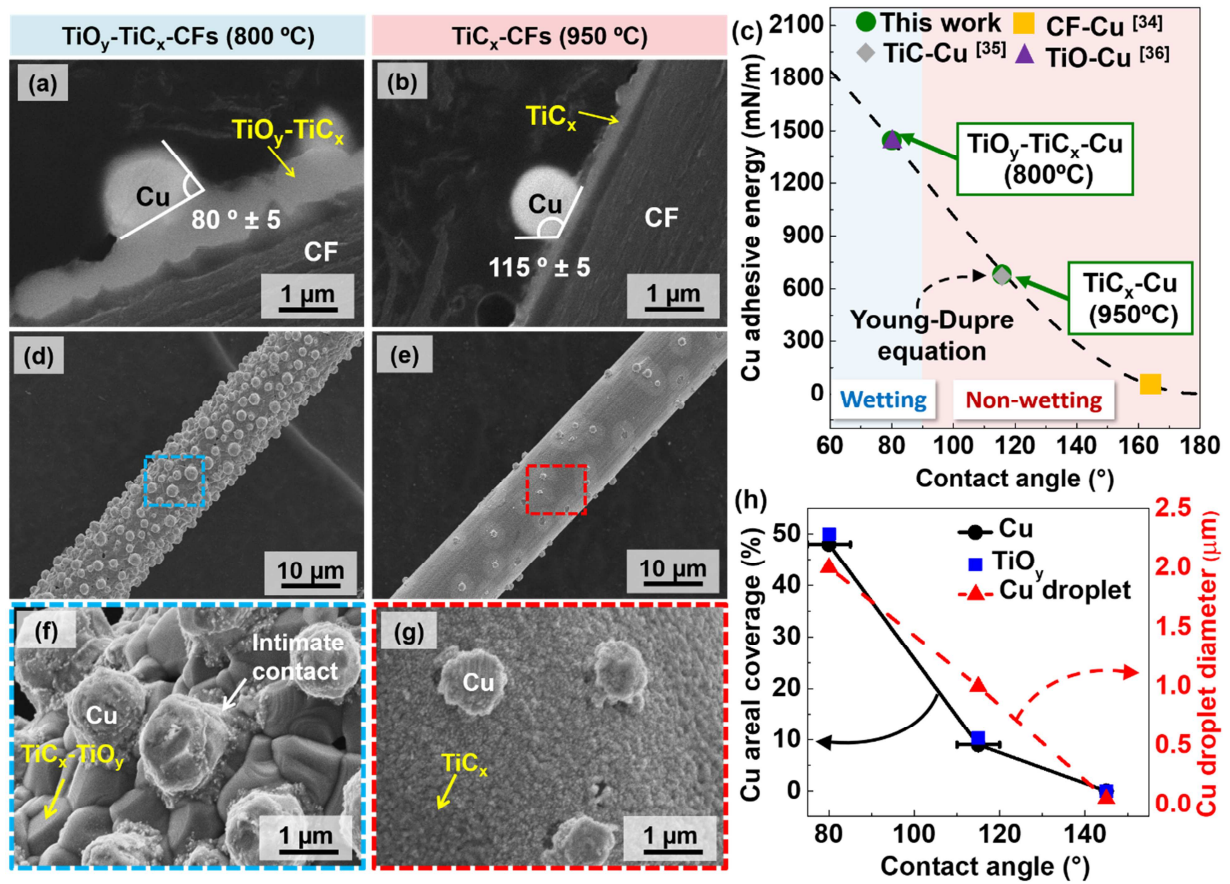


**Figure 5.** Cu contact angle measured on CFs coated with (a)  $\text{TiC}_x$  and (b)  $\text{TiO}_x\text{-TiC}_y$  prepared at 800 and 950 °C, respectively. (c) Adhesive (wetting) energy vs. contact angle measured in this work (●) compared to values reported by others for Cu on CF (■) [34], TiC (◆) [35], and TiO (▲) [36], SEM micrographs showing the wetting behavior of Cu on the coated CFs prepared at

(d), (e) 800 and (f), (g) 950 °C. (h) Measured Cu areal coverage with the equivalent TiO<sub>y</sub> content and droplet diameter as functions of the wetting angle.

The specific time,  $t_2$ , governing the rate of diffusion mass transport of Ti<sup>n+</sup> to the outer CFs surface (Step 2) was controlled by the viscosity of the KCl and the mean distance between the Ti<sup>0</sup> particles and the CFs. Assuming a statistical average distribution of particles, the mean interparticle distance was, conservatively, smaller than 100 μm. The approximate time for Ti<sup>n+</sup> to diffuse this distance,  $t_2$ , can be estimated from:

$$t_2 \sim \frac{\langle x \rangle^2}{2D_{Ti^{n+}}}. \quad (1)$$

**Equation (1)** gives an estimated time of  $t_2 < 10$  s to diffuse the 100 μm (mean Ti<sup>0</sup>/CF interparticle distance). The conclusion from the simple analyses is that both the particle dissolution (Step 1) and Ti<sup>n+</sup> diffusion mass transport (Step 2) are fast with Step 2 being the faster one.

In contrast to the time scale of a few minutes and seconds for Steps 1 and 2, respectively, the time scale for the coating process is on the order of hours. This leads to the logical conclusion that the process step governing the rate of coating formation is Step 3, the diffusion mass transport of Ti, and likely counter diffusion of C, through the interphase coating.

Semi-qualitative analyses of the XRD peak intensities of coated CFs were used to follow step 3, the TiC<sub>x</sub> formation rate versus time at temperatures of 800 and 950 °C, as presented in **Figures 6 (c) and (d)**, respectively. The integrated XRD peak intensities at 800 °C show the formation of TiC<sub>x</sub> even after 0.5 h, but associated with noticeable Ti peaks (**Figure 6 (c)**). The amount of Ti continuously decreases with the coating time. After 3 h of reaction, the Ti presents only in trace amounts while none is observed after 5 h (**Figure 6 (c)**). At 950 °C, essentially complete Ti

dissolution occurs after only 0.5 h, as evidenced by the absence of the Ti XRD peaks and the high  $\text{TiC}_x$  signal (**Figure 6 (d)**). These results support the above conclusion that mass transport diffusion through the coating is the rate-limiting process and strongly depends on the coating temperature. A slow diffusion and reaction rate at a low coating temperature favors the formation of non-stoichiometric  $\text{TiC}_x$ , in which the reactive Ti sites can be easily oxidized and subsequently results in a graded  $\text{TiO}_y\text{-TiC}_x$  coating that contributes better wetting to molten Cu.

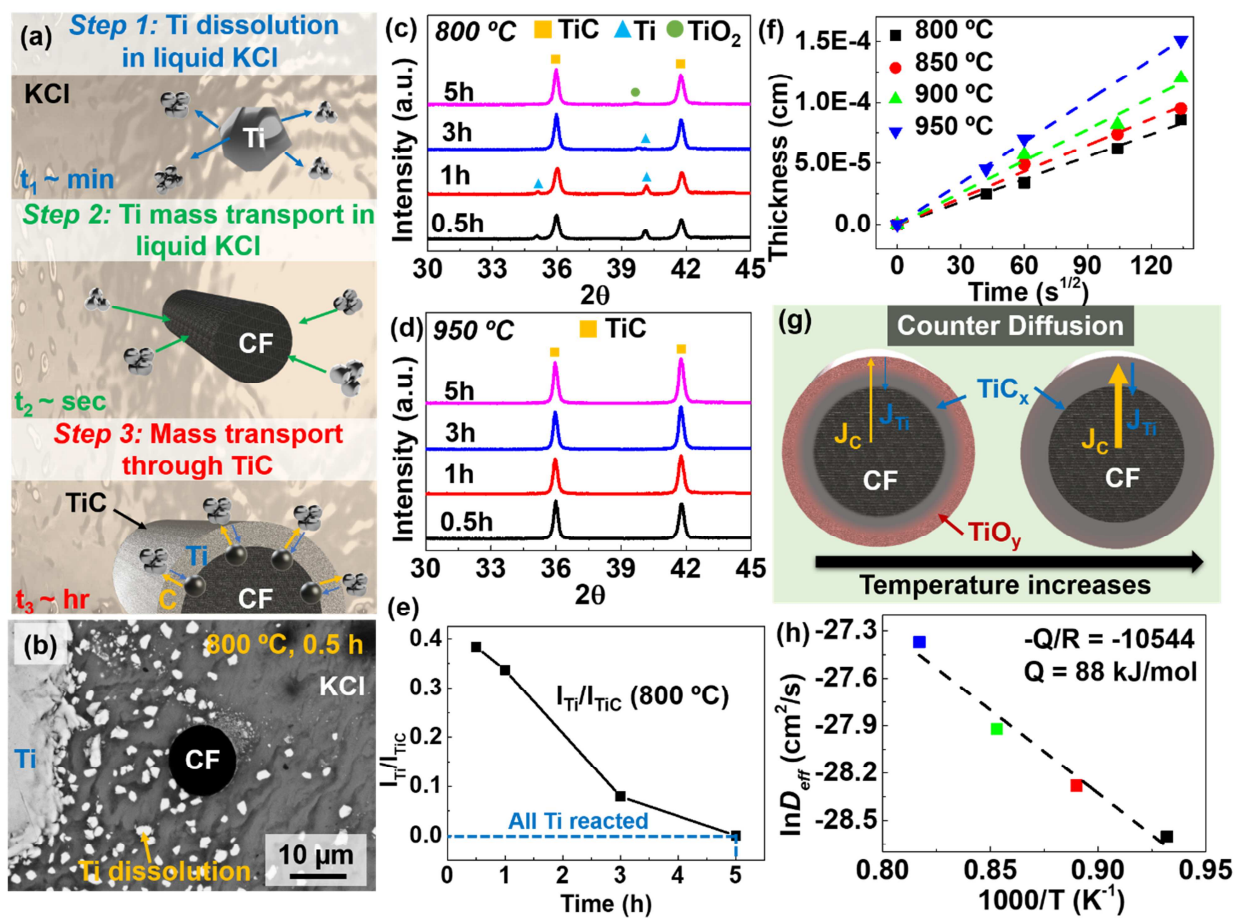


**Figure 6.** (a) Schematic of the three main steps of a molten-salt coating process, (b) SEM micrographs of rapidly quenched salt at  $800\text{ }^\circ\text{C}$  for  $0.5\text{ h}$ , XRD diffractograms of washed CFs for coating times ranging from  $0.5$  to  $5\text{ h}$  at (c)  $800\text{ }^\circ\text{C}$  and (d)  $950\text{ }^\circ\text{C}$ , and (e)  $I_{\text{Ti}}/I_{\text{TiC}}$  XRD ratio as functions of the coating time. (f) Coating thickness as a function of the square root of time for

different coating temperatures; **(g)** schematic representation of the temperature effect on the graded TiO<sub>y</sub>-TiC<sub>x</sub> coated layer; **(h)** Arrhenius plot of the natural log of  $D_{eff}$  versus the inverse of the coating temperature.

To evaluate the counter diffusion at different salt bath temperature, the coating thickness versus the coating time was monitored up to 5 h between 800 and 950 °C. As shown in the cross-sectional SEM images of the as-prepared coatings (supplemental **Figure S8**), the coating thickness increases as the coating time and temperature increases. Assuming the simplest case of one-dimensional diffusion mass transport of reactants (Ti and C) through the coated layer, the growth of the coating thickness can be described as a function of the square root of the coating time, using the following equation [39] :

$$x = a\sqrt{D_{eff}t}, \quad (2)$$

where  $x$  is the carbide coating thickness (cm),  $a$  is a unit-less proportionally constant (typically set to 2),  $t$  is the coating time (s), and  $D_{eff}$  is the effective diffusivity through the layer (cm<sup>2</sup>/s). As shown in **Figure 6 (f)**, the coating thickness ( $x$ ) shows a linear increase with the square root of the coating time in agreement with this simple treatment. The effective diffusivities,  $D_{eff}$ , at the different temperatures can be retrieved from the slopes of the curves. The  $D_{eff}$  increased with the coating temperature ranging from a value of  $3.8 \times 10^{-13}$  to  $1.3 \times 10^{-12}$  m<sup>2</sup>/s at 800 and 950 °C, respectively. These values reasonably agree with values reported by Koichiro Koyama *et al.* for the diffusion of C in TiC over a temperature range similar to that used in this work [40]. The evaluation of  $D_{eff}$  shows a carbon diffusion more than three-fold lower at 800 °C than at 950 °C. A slow C diffusion at a low coating temperature produces a more Ti-rich coating with more reactive non-bonded Ti sites, thus a higher oxide content in the coated layer as illustrated in **Figure 6 (g)**.

The  $D_{eff}$  is expected to show an Arrhenius temperature dependence [41,42] :

$$D_{eff} = D_0 e^{\frac{-Q_{eff}}{RT}}, \quad (3)$$

where  $D_0$  is the preexponential factor,  $Q_{eff}$  is the activation energy (J/mol) governing the overall intra-coating diffusion process, and  $R$  is the gas constant (J/mol.K). The  $Q_{eff}$  was determined to be ~88 KJ/mol by linear regression to the data in **Figure 6 (h)**. The activation energy is lower than the one reported by Knuth Albertsen *et al.* for grain boundary diffusion of C in bulk TiC below 1100 °C (174 kJ/mol) [43]; probably due to the enhancement grain boundary diffusion between bulk and coated TiC [43][44].

#### 4. CONCLUSION

In summary, tailor graded  $TiO_y-TiC_x$  coatings were synthesized on CFs. The  $TiO_y$  formation was observed after the dissolution of the molten salt in boiling water and is assumed to be the result of oxidation of reactive Ti sites near the exterior coated surface. The oxide-rich carbide coating shows significantly improved wettability by molten Cu compared to the oxide-carbide rich layer. Notably, the Cu wetting angle for the  $TiO_y-TiC_x$ -CF sample prepared at 800 °C was  $\sim 80^\circ \pm 5^\circ$  with a Cu surface coverage of ~50% versus  $\sim 115^\circ$  and ~ 10% for the  $TiC_x$ -CF sample made at 950 °C. CFs alone show mostly no Cu coverage.

By varying the reaction temperature (800-950 °C) and time (1-5 h) and using rapid thermal quenching, the formation mechanism was investigated. The results indicate a three-step process: 1) A short induction period controlled by rapid Ti dissolution in the molten salt, 2) rapid Ti mass transport in the molten salt and fast reaction at the CFs surface, and 3) mass transport through the layer that is controlled by a combination of titanium and carbon counter-diffusion.

Fabrication of a graded  $\text{TiO}_y\text{-TiC}_x$  coating on CF substrate via a molten salt process offers a simple way to tailor the properties of CFs. Thus, delivering an efficient route to optimize the properties of metal-carbon interphase.

Journal Pre-proof

## AUTHOR INFORMATION

### Author Contributions

‡ Loic Constantin and Dr. Lisha Fan contributed equally to this work. All authors approved the final version.

### Acknowledgment

The authors are gratefully for the financial support provided by the National Science Foundation (CMMI 1826392) and the Nebraska Center for Energy Sciences Research (NCESR). Also, the authors would like to thank Dr. John Campbell for helpful discussions and revisions on the manuscript.

## REFERENCES

- [1] M. Hasan, J. Zhao, Z. Jiang, Micromanufacturing of composite materials: a review, *Int. J. Extrem. Manuf.* 1 (2019) 012004. <https://doi.org/10.1088/2631-7990/ab0f74>.
- [2] S.J. Sun, M.D. Zhang, Interface characteristics and mechanical properties of carbon fibre reinforced copper composites, *Journal of Materials Science.* 26 (1991) 5762–5766. <https://doi.org/10.1007/BF01130112>.
- [3] J. Koráb, P. Štefánik, Š. Kavecký, P. Šebo, G. Korb, Thermal conductivity of unidirectional copper matrix carbon fibre composites, *Composites Part A: Applied Science and Manufacturing.* 33 (2002) 577–581. [https://doi.org/10.1016/S1359-835X\(02\)00003-9](https://doi.org/10.1016/S1359-835X(02)00003-9).
- [4] W. Buchgraber, G. Korb, T. Schubert, B. Kempf, Carbon Fibre Reinforced Copper Matrix Composites: Production Routes and Functional Properties, in: *Microstructural Investigation and Analysis*, Wiley-VCH Verlag GmbH & Co. KGaA, Weinheim, FRG, 2006: pp. 150–155. <https://doi.org/10.1002/3527606165.ch22>.
- [5] J.-F. Silvain, A. Veillère, Y. Lu, Copper-Carbon and Aluminum-Carbon Composites Fabricated by Powder Metallurgy Processes, *Journal of Physics: Conference Series.* 525 (2014) 012015. <https://doi.org/10.1088/1742-6596/525/1/012015>.
- [6] P. Hidalgo-Manrique, X. Lei, R. Xu, M. Zhou, I.A. Kinloch, R.J. Young, Copper/graphene composites: a review, *J Mater Sci.* 54 (2019) 12236–12289. <https://doi.org/10.1007/s10853-019-03703-5>.
- [7] A.B. Spierings, C. Leinenbach, C. Kenel, K. Wegener, Processing of metal-diamond-composites using selective laser melting, *Rapid Prototyping Journal.* (2015). <https://doi.org/10.1108/RPJ-11-2014-0156>.
- [8] L. Constantin, L. Fan, B. Mortaigne, K. Keramatnejad, Q. Zou, C. Azina, Y.F. Lu, J.-F. Silvain, Laser sintering of cold-pressed Cu powder without binder use, *Materialia.* 3 (2018) 178–181. <https://doi.org/10.1016/j.mtla.2018.08.021>.

- [9] K. Yoshida, H. Morigami, Thermal properties of diamond/copper composite material, *Microelectronics Reliability*. 44 (2004) 303–308. [https://doi.org/10.1016/S0026-2714\(03\)00215-4](https://doi.org/10.1016/S0026-2714(03)00215-4).
- [10] L. Xia, B. Jia, J. Zeng, J. Xu, Wear and mechanical properties of carbon fiber reinforced copper alloy composites, *Materials Characterization*. 60 (2009) 363–369. <https://doi.org/10.1016/J.MATCHAR.2008.10.008>.
- [11] Q. Kang, X. He, S. Ren, L. Zhang, M. Wu, C. Guo, W. Cui, X. Qu, Preparation of copper–diamond composites with chromium carbide coatings on diamond particles for heat sink applications, *Applied Thermal Engineering*. 60 (2013) 423–429. <https://doi.org/10.1016/J.APPLTHERMALENG.2013.05.038>.
- [12] C.R. Rambo, N. Travitzky, P. Greil, Conductive TiC/Ti–Cu/C composites fabricated by Ti–Cu alloy reactive infiltration into 3D-printed carbon performs, *Journal of Composite Materials*. 49 (2015) 1971–1976. <https://doi.org/10.1177/0021998314541307>.
- [13] X. QU, L. ZHANG, M. WU, S. REN, Review of metal matrix composites with high thermal conductivity for thermal management applications, *Progress in Natural Science: Materials International*. 21 (2011) 189–197. [https://doi.org/10.1016/S1002-0071\(12\)60029-X](https://doi.org/10.1016/S1002-0071(12)60029-X).
- [14] K. Chu, C. Jia, H. Guo, W. Li, Microstructure and thermal conductivity of Cu–B/diamond composites, *Journal of Composite Materials*. 47 (2013) 2945–2953. <https://doi.org/10.1177/0021998312460259>.
- [15] Th. Schubert, B. Trindade, T. Weißgärber, B. Kieback, Interfacial design of Cu-based composites prepared by powder metallurgy for heat sink applications, *Materials Science and Engineering: A*. 475 (2008) 39–44. <https://doi.org/10.1016/J.MSEA.2006.12.146>.
- [16] K. Chu, C. Jia, H. Guo, W. Li, On the thermal conductivity of Cu–Zr/diamond composites, *Materials & Design*. 45 (2013) 36–42. <https://doi.org/10.1016/J.MATDES.2012.09.006>.
- [17] Y. Zhang, H.L. Zhang, J.H. Wu, X.T. Wang, Enhanced thermal conductivity in copper matrix composites reinforced with titanium-coated diamond particles, *Scripta Materialia*. 65 (2011) 1097–1100. <https://doi.org/10.1016/j.scriptamat.2011.09.028>.
- [18] Z.J. Dong, X.K. Li, G.M. Yuan, Y. Cong, N. Li, Z.Y. Jiang, Z.J. Hu, Fabrication and oxidation resistance of titanium carbide-coated carbon fibres by reacting titanium hydride with carbon fibres in molten salts, *Thin Solid Films*. 517 (2009) 3248–3252. <https://doi.org/10.1016/j.tsf.2008.11.046>.
- [19] H.O. Pierson, *Handbook of refractory carbides and nitrides : properties, characteristics, processing, and applications*, Noyes Publications, 1996.
- [20] D.A. Mortimer, M. Nicholas, The wetting of carbon and carbides by copper alloys, *Journal of Materials Science*. 8 (1973) 640–648. <https://doi.org/10.1007/BF00561219>.
- [21] X. Li, Z. Dong, A. Westwood, A. Brown, R. Brydson, A. Walton, G. Yuan, Z. Cui, Y. Cong, Low-Temperature Preparation of Single Crystal Titanium Carbide Nanofibers in Molten Salts, *Crystal Growth & Design*. 11 (2011) 3122–3129. <https://doi.org/10.1021/cg200386d>.
- [22] T. Kimura, Molten Salt Synthesis of Ceramic Powders, in: *Advances in Ceramics - Synthesis and Characterization, Processing and Specific Applications*, InTech, 2011. <https://doi.org/10.5772/20472>.
- [23] X. Liu, Z. Wang, S. Zhang, Molten Salt Synthesis and Characterization of Titanium Carbide-Coated Graphite Flakes for Refractory Castable Applications, *International Journal*

- of Applied Ceramic Technology. 8 (2011) 911–919. <https://doi.org/10.1111/j.1744-7402.2010.02529.x>.
- [24] A. Le Bail, H. Duroy, J.L. Fourquet, Ab-initio structure determination of LiSbWO<sub>6</sub> by X-ray powder diffraction, *Materials Research Bulletin*. 23 (1988) 447–452. [https://doi.org/10.1016/0025-5408\(88\)90019-0](https://doi.org/10.1016/0025-5408(88)90019-0).
- [25] Q. Liu, X.-B. He, S.-B. Ren, T. Liu, Q.-P. Kang, X.-H. Qu, Effect of titanium carbide coating on the microstructure and thermal conductivity of short graphite fiber/copper composites, *J Mater Sci*. 48 (2013) 5810–5817. <https://doi.org/10.1007/s10853-013-7373-y>.
- [26] Z.J. Dong, X.K. Li, G.M. Yuan, Z.W. Cui, Y. Cong, A. Westwood, Tensile strength, oxidation resistance and wettability of carbon fibers coated with a TiC layer using a molten salt method, *Materials & Design*. 50 (2013) 156–164. <https://doi.org/10.1016/j.matdes.2013.02.084>.
- [27] E. Morton, R.K. Lewis, CONTRACT NO. NAW-663 FINAL REPORT PROPERTIES OF NON-STOICHIOMETRIC METALLIC CARBIDES, Mendeley. (n.d.). <https://www.mendeley.com/catalogue/contract-naw663-final-report-properties-nonstoichiometric-metallic-carbides/> (accessed February 6, 2019).
- [28] N. Frage, L. Levin, E. Manor, R. Shneck, J. Zabicky, Iron-titanium-carbon system. II. Microstructure of titanium carbide (TiC<sub>x</sub>) of various stoichiometries infiltrated with iron-carbon alloy, *Scripta Materialia*. 35 (1996) 799–803. [https://doi.org/10.1016/1359-6462\(96\)00230-8](https://doi.org/10.1016/1359-6462(96)00230-8).
- [29] J. Roger, B. Gardiola, J. Andrieux, J.-C. Viala, O. Dezellus, Synthesis of Ti matrix composites reinforced with TiC particles: thermodynamic equilibrium and change in microstructure, *Journal of Materials Science*. 52 (2017) 4129–4141. <https://doi.org/10.1007/s10853-016-0677-y>.
- [30] E. Fryt, Defect mobility in TiC<sub>1-x</sub> at high temperatures, *Solid State Ionics*. 101–103 (1997) 437–443. [https://doi.org/10.1016/S0167-2738\(97\)00139-2](https://doi.org/10.1016/S0167-2738(97)00139-2).
- [31] I. Dahan, U. Admon, N. Frage, J. Sariel, M.P. Dariel, Diffusion in Ti/TiC multilayer coatings, *Thin Solid Films*. 377–378 (2000) 687–693. [https://doi.org/10.1016/S0040-6090\(00\)01282-7](https://doi.org/10.1016/S0040-6090(00)01282-7).
- [32] S. Sarian, Diffusion of <sup>44</sup>Ti in TiC<sub>x</sub>, *Journal of Applied Physics*. 40 (1969) 3515–3520. <https://doi.org/10.1063/1.1658229>.
- [33] T. Matsumoto, H. Fujii, T. Ueda, M. Kamai, K. Nogi, Measurement of surface tension of molten copper using the free-fall oscillating drop method, *Meas. Sci. Technol*. 16 (2005) 432–437. <https://doi.org/10.1088/0957-0233/16/2/014>.
- [34] B. Kong, J. Ru, H. Zhang, T. Fan, Enhanced wetting and properties of carbon/carbon-Cu composites with Cr<sub>3</sub>C<sub>2</sub> coatings by Cr-solution immersion method, *Journal of Materials Science & Technology*. 34 (2018) 458–465. <https://doi.org/10.1016/j.jmst.2017.01.028>.
- [35] D.A. Mortimer, M. Nicholas, The wetting of carbon and carbides by copper alloys, *J Mater Sci*. 8 (1973) 640–648. <https://doi.org/10.1007/BF00561219>.
- [36] N. Eustathopoulos, B. Drevet, Interfacial bonding, wettability and reactivity in metal/oxide systems, *Journal de Physique III*. 4 (1994) 1865–1881. <https://doi.org/10.1051/jp3:1994244>.
- [37] H. Sekimoto, Y. Nose, T. Uda, H. Sugimura, Quantitative Analysis of Titanium Ions in the Equilibrium with Metallic Titanium in NaCl-KCl Equimolar Molten Salt, *MATERIALS TRANSACTIONS*. 51 (2010) 2121–2124. <https://doi.org/10.2320/matertrans.M2010238>.

- [38] W.C. Kreye, H.H. Kellogg, The Equilibrium between Titanium Metal,  $TiCl_2$ , and  $TiCl_3$  in  $NaCl \square KCl$  Melts, *J. Electrochem. Soc.* 104 (1957) 504–508. <https://doi.org/10.1149/1.2428636>.
- [39] C.R. Clayton, *Materials science and engineering: An introduction, Materials Science and Engineering*. 94 (n.d.) 266–267. [https://www.academia.edu/8089620/Materials\\_Science\\_and\\_Engineering\\_An\\_Introduction\\_EIGHTH\\_EDITION\\_by\\_William\\_D.\\_Callister\\_Jr\\_and\\_David\\_G.\\_Rethwisch](https://www.academia.edu/8089620/Materials_Science_and_Engineering_An_Introduction_EIGHTH_EDITION_by_William_D._Callister_Jr_and_David_G._Rethwisch) (accessed June 13, 2019).
- [40] K. Koyama, Y. Hashimoto, S. Omori, Diffusion of Carbon in  $TiC$ , *Trans. JIM*. 16 (1975) 211–218. <https://doi.org/10.2320/matertrans1960.16.211>.
- [41] T. Arai, Carbide coating process by use of molten borax bath in Japan, *Journal of Heat Treating*. 1 (1979) 15–22. <https://doi.org/10.1007/BF02833234>.
- [42] J. Roger, F. Audubert, Y. Le Petitcorps, Thermal reaction of  $SiC$  films with tungsten and tungsten–rhenium alloys, *Journal of Materials Science*. 43 (2008) 3938–3945. <https://doi.org/10.1007/s10853-007-2334-y>.
- [43] K. Albertsen, H.-J. Schaller, Diffusion of C in  $TiC$ , *Berichte Der Bunsengesellschaft Für Physikalische Chemie*. 98 (1994) 1224–1230. <https://doi.org/10.1002/bbpc.19940981003>.
- [44] D.D. Himbeault, R.A. Varin, K. Piekarski, Carbon fibers coated with chromium carbide using the liquid metal transfer agent technique, *MTA*. 20 (1989) 165–170. <https://doi.org/10.1007/BF02647503>.

### Declaration of interests

The authors declare that they have no known competing financial interests or personal relationships that could have appeared to influence the work reported in this paper.



Yongfeng Lu, PhD

Lott Distinguished Professor of Electrical and Computer Engineering, Mechanical and Materials Engineering

SPIE, LIA, OSA, and IAPLE Fellow

Past President, International Academy of Photonics and Laser Engineering (IAPLE, UK).

Past President, Laser Institute of America (LIA, USA)

Editor-in-Chief, Journal of Laser Applications (LIA and AIP, USA)

International Editor-in-Chief, International Journal of Extreme Manufacturing

419 Nebraska Hall,

University of Nebraska Lincoln,

Lincoln, NE 68588-0511.

Tel: 402-472-8323; Cell: 402-617-3509; Fax: 402-472-4732

Email: [ylu2@unl.edu](mailto:ylu2@unl.edu)